

Strong-motion characteristics of January and February 2001 earthquakes in El Salvador

J.M. Cepeda*

Dpto. de Mecánica Estructural, Universidad Centroamericana "José Simeón Cañas" (UCA), A.P. (01) 168, San Salvador, El Salvador

M.B. Benito

Universidad Politécnica de Madrid (UPM), Madrid, Spain

E.A. Burgos

Dpto. de Mecánica Estructural, Universidad Centroamericana "José Simeón Cañas" (UCA), A.P. (01) 168, San Salvador, El Salvador

ABSTRACT

During 2001, very intense seismic activity occurred in El Salvador and concentrated in the in-slab subduction zone and the volcanic chain that runs along the central part of the country from west to east. The ground motions of 188 earthquakes were recorded by 31 accelerographs, which produced a total of 479 records. The purpose of this paper is to present the main characteristics of this strong-motion database and to examine the horizontal ground motion attenuation of earthquakes that occurred in both seismic zones. Even though the database is not complete in terms of magnitude, and site conditions are only known for 2% of the records, an application is carried out by making adjustments of attenuation equations derived from worldwide data. The analysis of the subduction earthquake records shows that the attenuation characteristics of the El Salvador 2001 database seem to have a better agreement with interface-type events rather than with the in-slab type of earthquakes assumed in the present study. The attenuation analysis of the shallow upper crustal events indicates that rupture directivity effects may be relevant and should deserve attention in future assessments of strong ground motion.

Keywords: earthquakes, strong-motion records, peak ground acceleration, response spectral ordinates, attenuation equations.

INTRODUCTION

During January and February 2001, two large earthquakes struck El Salvador, causing major destruction mainly due to widespread landslides and collapse of nonengineered structures. The 7.7 M_w first event occurred on January 13 and had its origin in the in-slab subduction zone that results from the convergence of the subducting Cocos plate under the Caribbean plate. The second event on February 13, 6.6 M_w , was associated with an

inland crustal fault. These events were accompanied by intense activity in both source areas. The parameters, focal mechanism, and other source characteristics of these events and their distribution in space and time are detailed in Benito et al. (this volume, Chapter 25). The seismic sources and parameters used in the present study, as well as the magnitude conversions (from M_c to M_w), are based on the above reference. Bommer et al. (2002) have previously presented an overall assessment of the January and February 2001 main shocks, including an assessment of the strong-motion attenuation characteristics of these earthquakes.

*jcepeda@ing.uca.edu.sv

Cepeda, J.M., Benito, M.B., and Burgos, E.A., 2004, Strong-motion characteristics of January and February 2001 earthquakes in El Salvador, *in* Rose, W.I., Bommer, J.J., López, D.L., Carr, M.J., and Major, J.J., eds., *Natural hazards in El Salvador*: Boulder, Colorado, Geological Society of America Special Paper 375, p. 405–421. For permission to copy, contact editing@geosociety.org. © 2004 Geological Society of America

The seismic activity during 2001 in El Salvador was recorded on 31 accelerographs of three strong-motion networks: the government network operated by SNET (Servicio Nacional de Estudios Territoriales, formerly CIG, Centro de Investigaciones Geotécnicas), and two private networks operated by GESAL (Geotérmica Salvadoreña) and UCA (Universidad Centroamericana “José Simeón Cañas”). Bommer et al. (1997) and Cepeda et al. (1997a) present the design and characteristics of the UCA network. Table 1 gives information on how to obtain the data produced by these three networks.

These strong-motion networks produced records for the main events and the aftershock series. A total of 479 triaxial records from 188 earthquakes in 2001 were collected and analyzed for the present study. Figure 1 shows the epicenters of these 188 earthquakes as well as the locations of the 31 strong-motion stations. The source parameters of the events were taken from the SNET catalog of 2001. The source parameters of the January 13 and February 13

earthquakes were taken from the PDE (Preliminary Determination of Epicenters) catalog of the U.S. Geological Survey (USGS). The geographical coordinates for the strong-motion stations and the number of records in each station are presented in Tables 2 and 3. Prior to the January and February 2001 earthquakes, a major part of the strong-motion records for large earthquakes ($M \geq 6$) in Central America were obtained from the March and April 1990 earthquakes in Costa Rica (Cepeda et al., 1997a).

The purpose of this paper is to assess attenuation characteristics of the subduction and volcanic chain (shallow upper crustal) earthquakes respectively, based on the strong-motion records of 2001.

SELECTION OF SEISMIC SOURCES

The definition of the source-site distance of the attenuation models is determined by the type of seismic source. For moderate-

TABLE 1. WEB AND E-MAIL ADDRESSES FOR OBTAINING 2001 STRONG-MOTION DATA

Owner of instruments	Web addresses of institution or link for downloading data	Contact persons	E-mail addresses
SNET	www.snet.gob.sv nsmp.wr.usgs.gov/data_sets/20010113_1.html	Griselda Marroquín Douglas Hernández	gmarroquin@snet.gob.sv dherandez@snet.gob.sv
GESAL	www.gesal.com.sv	José Rivas	jarivas@gesal.com.sv
UCA	www.uca.edu.sv	Reynaldo Zelaya José Cepeda	rezelaya@ing.uca.edu.sv jcepeda@ing.uca.edu.sv

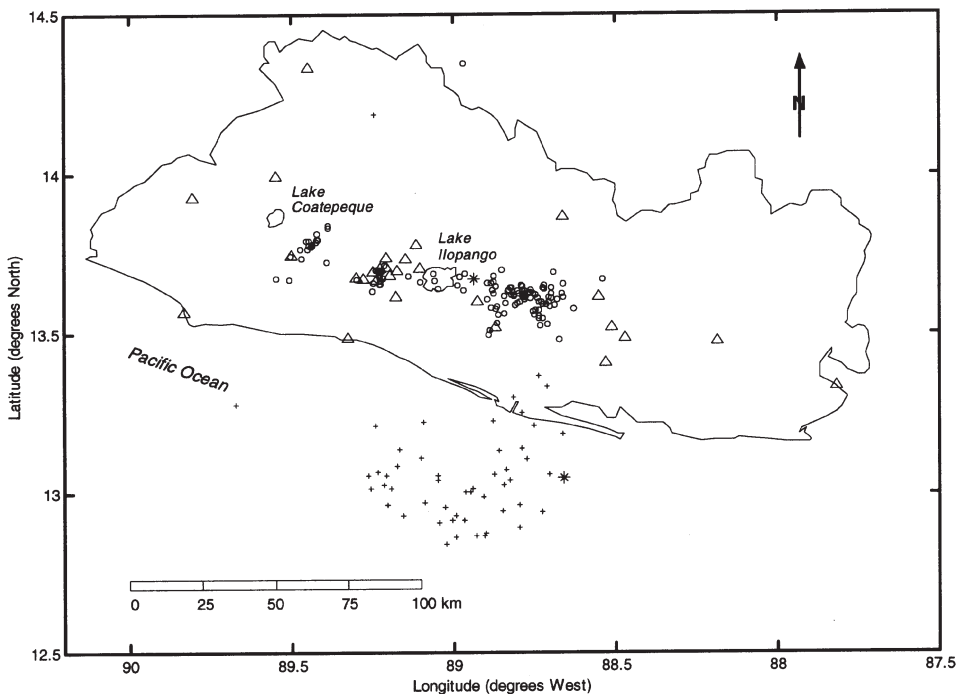


Figure 1. Map of El Salvador showing epicenters of events that produced strong-motion records during 2001. Crosses—subduction earthquake epicenters. Circles—shallow upper crustal earthquake epicenters. Stars—epicenters of the January 13 (southern star) and February 13 (northern star) earthquakes. Triangles—strong-motion stations that recorded at least one earthquake.

TABLE 2. CHARACTERISTICS OF STRONG MOTION RECORDING STATIONS

Code	Description	Owner	Latitude (°N)	Longitude (°W)	Instrument
AH	Ahuachapán	CIG	13.925	89.805	SMA-1
AR	Armenia	UCA	13.744	89.501	SSA-2
BA	San Bartolo	UCA	13.704	89.106	SSA-2
BE	Berlin	GESAL	13.497	88.529	SSA-2
CA	CEPA, Acajutla	CIG	13.567	89.833	SMA-1
CI	Centro de Investigaciones Geotécnicas, San Salvador	CIG	13.698	89.173	SMA-1
CM	CESSA, Metapán	CIG	14.333	89.450	SMA-1
CU	Cutuco	CIG	13.333	87.817	SMA-1
DB	Ciudadela Don Bosco, Soyapango	CIG	13.733	89.150	SMA-1
EX	Externado, San Salvador	UCA	13.707	89.207	SSA-2
LI	La Libertad	UCA	13.486	89.327	SSA-2
MG	San Miguel	CIG	13.475	88.183	SMA-1
NO	San Pedro Nonualco	UCA	13.602	88.927	SSA-2
OB	Observatorio, San Salvador	CIG	13.681	89.198	SMA-1
PA	Panchimalco	UCA	13.614	89.179	SSA-2
QC	"15 de septiembre" dam (zero level)	CIG	13.616	88.550	SMA-1
RF	Relaciones Exteriores (bottom of borehole)	CIG	13.692	89.250	SMA-1
RS	Relaciones Exteriores (ground level)	CIG	13.692	89.250	SMA-1
SA	Santa Ana	CIG	13.992	89.550	SMA-1
SE	Sensuntepeque	CIG	13.867	88.663	SMA-1
SM	Santiago de María	CIG	13.486	88.471	SMA-1
SS	Seminario "San José de La Montaña" (ground level), San Salvador	CIG	13.705	89.225	SMA-1
ST	Santa Tecla	CIG	13.675	89.300	SMA-1
TE	Hospital San Rafael, Santa Tecla	UCA	13.671	89.279	SSA-2
TO	Tonacatepeque	UCA	13.778	89.114	SSA-2
TR	Planta Boca Pozo (TR-9), Berlín	GESAL	13.520	88.512	SSA-2
UC	Universidad Centroamericana, Antiguo Cuscatlán	CIG	13.677	89.236	SMA-1
VF	Viveros de DUA (bottom of borehole), San Salvador	CIG	13.737	89.209	SMA-1
VI	San Vicente	UCA	13.642	88.784	SSA-2
VS	Viveros de DUA (ground level), San Salvador	CIG	13.737	89.209	SMA-1
ZA	Zacatecoluca	UCA	13.517	88.869	SSA-2

size events, the use of hypocentral or epicentral distance, i.e., point modeling of the source, is appropriate when the dimensions of the rupture are small compared to the source-site distance. This is not the case for large-magnitude events. In the following sections, two earthquake cases are discussed: January 13 and February 13.

January 13 Earthquake

The source parameters of this earthquake reported by NEIC (National Earthquake Information Center) are origin time, 17:33:32.38 u.t.; coordinates of epicenter, 13.049° N and 88.660° W; focal depth, 60 km; and reported magnitudes of 6.4 m_b , 7.8 M_s , and 7.7 M_w . The effect of source dimensions on the recorded motions has been examined by Cepeda (2001a). The vertical component was used in order to minimize the effects of amplification (or deamplification) due to topographic or geologic features. A very large scatter was observed when peak

vertical acceleration was plotted against hypocentral distance. This fact can be partially explained if the source dimensions are taken into account. For such a major earthquake, whose rupture extended along a large portion of the Salvadoran coastline, it is clear that source dimensions and source-site distances for the strong-motion station are comparable. Hence, point modeling for the source does not seem to be adequate for this event. In the following paragraphs the use of a rupture plane as the event source is examined.

Consistent with the strike and dip angle of the rupture plane defined by Benito et al. (this volume, Chapter 25), a robust fit was performed for the main event and the aftershocks within two days after the main shock (Lay and Wallace, 1995). The distribution of aftershocks and the USGS solution for the main shock are shown in Figure 2. For the regression, only events in the epicentral area were taken as aftershocks.

The fit yields the following result:

TABLE 3. GEOLOGY OF STATIONS AND NUMBER OF RECORDS

Code	Geology [§]	Description	Subduction Records	Shallow Upper Crustal Records	NEHRP Site
AH	s3	Acid pyroclastites, volcanic epiclastites ("brown tuffs")*	1	N.D.	D
AR	s3	Acid pyroclastites, volcanic epiclastites ("brown tuffs")*	28	23	D
BA	s4	Acid pyroclastites ("white earth")*	20	17	D
BE	s2	Andesitic and basaltic effusives: piroclastites*	N.D.	1	D
CA	b1	Volcanic epiclastites, pyroclastites, lava flows*	1	N.D.	Rock
CI	s5'a	Basaltic and andesitic lavas, predominantly from San Salvador volcano [#]	N.D.	2	Rock
CM	Q'f	Alluvium, locally with pyroclastites*	1	N.D.	Rock
CU	c3	Andesitic-basaltic effusives*	1	N.D.	Rock
DB	s4	Volcanic ashes ("white earth"), low consolidated [#]	1	2	D
EX	s4	Volcanic ashes ("white earth"), low consolidated [#]	17	16	D
LI	Q'f	Alluvium, locally with pyroclastites*	29	5	C
MG	s3	Acid pyroclastites, volcanic epiclastites ("brown tuffs")*	1	N.D.	C
NO	c1	Acid pyroclastites, volcanic epiclastites, welded tuffs*	33	4	D
OB	s4	Volcanic ashes ("white earth"), low consolidated [#]	1	2	D
PA	c1	Acid pyroclastites, volcanic epiclastites, welded tuffs*	8	10	Rock
QC	b3	Andesitic-basaltic effusives*	1	1	Rock
RF	s3'a	"Brown tuffs," locally with ashes and scoria [#]	1	1	C
RS	s3'a	"Brown tuffs," locally with ashes and scoria [#]	1	1	D
SA	s3	Acid pyroclastites, volcanic epiclastites ("brown tuffs")*	1	N.D.	D
SE	b1	Volcanic epiclastites, pyroclastites, lava flows*	1	N.D.	Rock
SM	s3	Acid pyroclastites, volcanic epiclastites ("brown tuffs")*	1	N.D.	D
SS	s4	Volcanic ashes ("white earth"), low consolidated [#]	1	1	D
ST	s3	Acid pyroclastites, volcanic epiclastites ("brown tuffs")*	1	1	D
TE	s2	Andesitic and basaltic effusives: piroclastites*	29	13	C
TO	c1	Acid pyroclastites, volcanic epiclastites, welded tuffs *	24	23	D
TR	s2	Andesitic and basaltic effusives: piroclastites*	1	N.D.	D
UC	s3'a	"Brown tuffs," locally with ashes and scoria [#]	N.D.	2	D
VF	s4	Volcanic ashes ("white earth"), low consolidated [#]	N.D.	2	C
VI	s4	Acid pyroclastites ("white earth")*	21	65	D
VS	s4	Volcanic ashes ("white earth"), low consolidated [#]	1	2	D
ZA	b1	Volcanic epiclastites, pyroclastites, lava flows*	28	31	Rock
TOTAL			254	225	

Note: N.D.—no data

N.A.—not applicable

§—symbols used in the geologic map of El Salvador

*—Obtained from El Salvador geologic map 1:500,000

#—Obtained from San Salvador geologic map 1:15,000

C—NEHRP soil type C

D—NEHRP soil type D

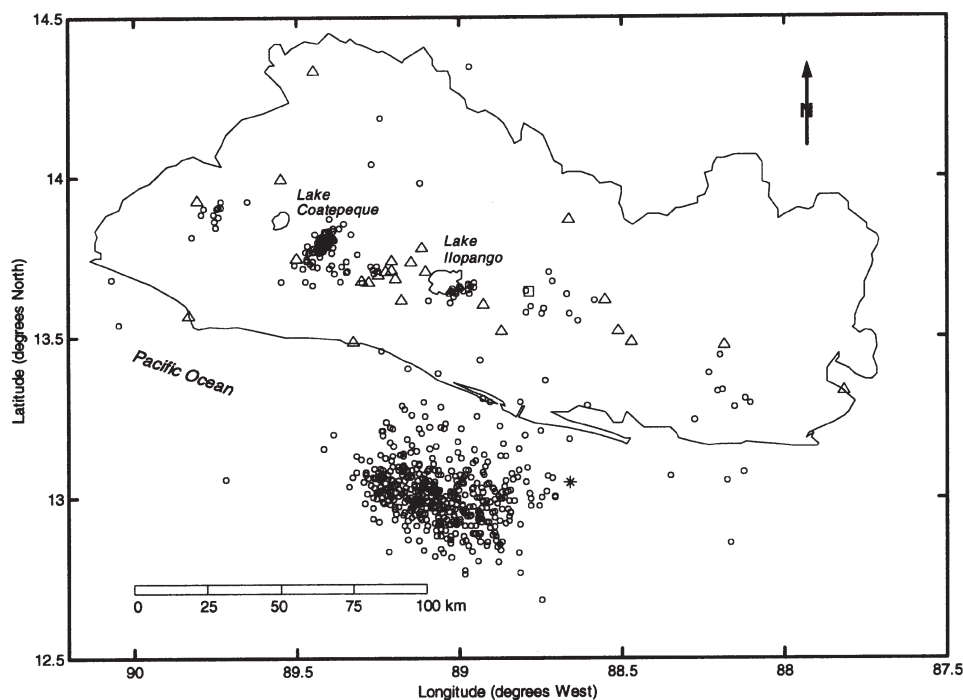


Figure 2. Map of El Salvador showing epicenter of the January 13 main shock (star) and epicenters of earthquakes (circles) that occurred within a two-day period after the main shock. Triangles—strong-motion stations that recorded the January 13 earthquake. Square—station VI.

$$\text{Depth} = 482699 - 0.339032 \text{ Longitude} - 1.69855 \text{ Latitude} \quad (1)$$

where *Depth*, *Longitude*, and *Latitude* are in meters, and the projection used for these coordinates is Lambert NAD 27. This projection is used in order to be consistent with the convention of the existing geographical data for El Salvador.

The strike angle of the calculated plane is 281.3°, and the dip angle was fixed to 60° according to the fracture plane solution given by Benito et al. (this volume, Chapter 25). Both the strike and dip angles closely agree with the fault plane solution, which is a normal fault due to a rupture of the subducting Cocos plate oceanic crust. The borders of the rupture plane are constrained by the distribution of aftershocks.

In Table 4, the trend of peak vertical acceleration versus distance to rupture surface presents a more consistent trend, showing that this parameter of distance agrees more adequately with the ground-motion attenuation behavior.

February 13 Earthquake

The source parameters of this earthquake reported by NEIC (National Earthquake Information Center) are origin time, 14:22:05.82 u.t.; coordinates of epicenter, 13.671° N and

88.938° W; focal depth, 10 km; and the magnitudes reported are 5.5 m_b , 6.5 M_s , and 6.6 M_w . Using the Wells and Copper-smith (1994) relations, the rupture length was estimated to be 21.6 km, and the range of epicentral distances for the recording stations is between 78.7% and 284.3% of the above estimated length, which indicates that the source-site distances are comparable to the source dimensions, and therefore it is possible to anticipate that a point model of the source may not be adequate for the calculation of distances in the attenuation analysis.

The conditions for a fit to a rupture plane using the distribution of aftershocks are very poor in this case. The reason is that the high density and very close spacing of mapped geological faults in the surroundings of the epicentral area makes the task of assigning every event to a single fault almost impossible.

In order to better determine the fault rupture, the procedure described by Cepeda (2001b) was followed. The alignment and length of local faults were identified on a 1:100,000 geological map of El Salvador and compared with the strike of the focal mechanism presented by Benito et al. (this volume) and the above estimate of rupture length. A good agreement was found with the fault shown in Figure 3B, and this fault has been used as the earthquake source. The length of the surface trace of this fault is 23.7 km, compared to the 21.6 km given by the

TABLE 4. RECORDS FOR JANUARY 13, 2001 EARTHQUAKE:
PEAK ACCELERATION, PEAK VELOCITY AND PSEUDOSPECTRAL ACCELERATIONS FOR 0.3 s AND 1.0 s

Code	Rupture distance (km)	North-South				Vertical		East-West			
		PGA (cm/s ²)	PGV (cm/s)	PSA T = 0.3 s (cm/s ²)	PSA T = 1 s (cm/s ²)	PGA (cm/s ²)	PGV (cm/s)	PGA (cm/s ²)	PGV (cm/s)	PSA T = 0.3 s (cm/s ²)	PSA T = 1 s (cm/s ²)
LI	61.3	1092	53.2	1290	285	604	15.9	564	35.5	958	237
ZA	72.0	255	12.3	362	140	247	8.6	305	19.1	410	229
PA	75.4	173	9.2	223	174	87	7.3	151	9.4	182	111
SM	77.7	864	27.8	1607	350	432	16.1	702	40.4	2011	415
NO	78.9	569	37.5	1063	402	430	18.2	479	26.4	1789	319
TE	79.2	486	57.0	1103	385	239	18.5	477	34.2	1112	389
TR	79.4	453	18.6	1017	163	235	18.0	364	24.2	1279	220
ST	79.4	588	60.5	1119	514	464	21.6	761	43.3	2570	343
RF	81.0	204	19.5	476	233	184	13.9	205	16.6	470	251
RS	81.0	317	27.6	1207	280	323	15.3	298	22.9	1026	268
OB	81.4	420	38.4	1096	555	301	13.0	372	26.2	1052	507
SS	83.2	267	15.0	544	211	157	11.3	247	20.3	656	330
EX	83.7	295	25.4	962	441	151	11.9	273	17.4	584	394
BA	85.2	154	25.2	615	491	163	15.2	195	31.2	485	454
CA	86.5	106	18.6	209	282	49	4.2	96	14.6	226	183
VS	86.5	301	21.9	N.D.	N.D.	207	12.5	306	37.3	N.D.	N.D.
DB	87.1	221	23.2	473	523	157	11.3	245	19.2	502	183
QC	87.2	149	23.5	365	209	120	10.2	183	16.0	574	163
AR	87.3	589	49.6	751	1050	219	19.6	445	53.3	1183	657
MG	91.9	118	12.1	215	252	88	6.0	133	12.8	204	225
TO	92.0	258	23.1	594	424	201	9.8	230	23.2	611	208
SE	108.7	81	8.5	213	115	57	6.2	60	9.1	190	71
SA	112.1	133	19.5	373	407	50	6.2	84	13.6	169	175
CU	113.6	76	13.8	205	100	62	4.0	78	8.6	179	149
AH	114.8	210	16.6	335	335	121	10.8	143	14.9	318	324
CM	144.1	14	1.7	23	18	N.D.	N.D.	12	2.2	21	25

Note: Stations ordered with increasing rupture distance.

Rupture distance—distance to plane of rupture; PGA—horizontal peak ground acceleration; PGV—horizontal peak ground velocity; PSA—pseudospectral acceleration; T—period; N.D.—No data.

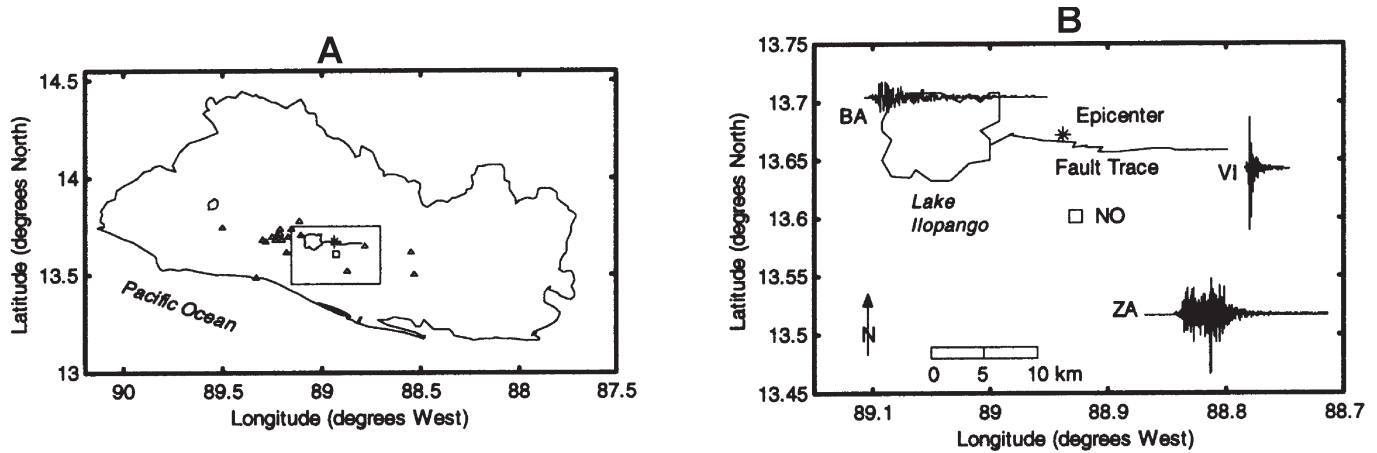


Figure 3. A: Map of El Salvador showing epicenter of the February 13 main shock (star) and strong-motion stations that produced records (triangles). Square—station NO. Rectangle marks the epicentral area, which is expanded in part B of this figure. B: Map of epicentral region of the February 13 earthquake. Star—epicenter. Square—station NO. North-south acceleration time histories are presented for stations BA, VI, and ZA.

empirical estimate. The E-W alignment of the surface trace matches closely the strike angle deduced from the focal mechanism. Since the reported dip angle is steep, the fault trace is approximated by the vertical projection of the rupture surface. In the following sections, for each recording station, the source to site distance reported for this event is the shortest horizontal distance to the fault trace shown in Figure 3.

Cepeda (2001b) presents an additional feature of the February 13 earthquake. This feature is an effect of strong-motion directivity, which is particularly observed in the recorded ground motions in the surroundings of the fault trace. In Figure 3B, if a west-east unilateral direction of the rupture is assumed, the expected acceleration time histories at VI (in the rupture direction) should show very high frequencies and large amplitudes, whereas the signal at BA (opposite to the rupture direction) should have low amplitudes and a low frequency content. It is assumed that the geologic conditions in VI and BA are not very different and hence are not expected to have a strong influence in the ground motions. These trends are confirmed after comparing with the observed ground motions. Figure 3B shows the north-south component for both stations. This figure also shows the trace recorded at ZA. The envelope of this record appears to indicate a multiple rupture of the fault. This same envelope was also observed at PA, which has almost the same latitude as NO and is slightly to the west of the limits of the window shown in Figure 3B.

CHARACTERISTICS OF STRONG-MOTION RECORDING STATIONS

Tables 2 and 3 show the characteristics of the strong-motion stations and instruments. The geology has been obtained from the digital versions of the 1:500,000 geological map of El Salvador

and the 1:15,000 geological map of San Salvador, digitized and geographically referenced by Brizuela and Menjivar (2001). When a site was found in both maps, the classification and description was taken from the 1:15,000 map of San Salvador. Each station was assigned a National Earthquake Hazard Reduction Program (NEHRP) site class (see Dobry et al., 2000), which is listed in the last column of Table 3. The NEHRP site class is originally calculated as the average shear wave velocity within the top 30 m (FEMA, 1997). Rock sites have average velocities of 760 m/s to 1500 m/s. NEHRP C sites are very dense soils or soft rocks with average velocities of 360 m/s to 760 m/s, and NEHRP D sites are defined as stiff soils with average velocities of 180 m/s to 360 m/s.

Very limited geotechnical information was available from the stations in order to make direct assignments of site classes. Standard Penetration Test blow counts were made available in stations RS, SS, and VS by SNET. Shear wave velocity profiles for stations CI and UC are presented by Italtেকna-Italconsult (1987). Hence, site classification according to NEHRP was directly made only for the above five stations. For the rest of the stations, which produced 98% of the records, the assignment of a site class was made indirectly based on a combination of the following indicators: the surface geology as indicated by the geologic maps, the shear wave velocities reported by Italtেকna-Italconsult (1987) for different types of volcanic materials in El Salvador, and the distribution of residuals at every station in a preliminary strong-motion attenuation analysis assuming uniform site conditions in all stations. The third indicator was considered only in the stations of the UCA network, because the number of records was considered significant and the average values of residuals were assumed to reflect the geologic site conditions.

Figures 2 and 3 show the distribution of recording stations for the January 13 and February 13 earthquakes.

PROCESSING OF RECORDS

The type and number of records used in the present study were 32 analogue records from SMA-1 instruments and 447 digital records from SSA-2 accelerographs.

The SMA-1 film records from the January 13 earthquake were processed by the USGS, and the rest of the SMA-1 records were processed by SNET. The analogue-to-digital conversion was performed by digitizing the original record from film.

The SSA-2 digital records produced by the GESAL and UCA networks were processed for this study using the Strong Motion Analyst software by Kinemetrics. The processing of the SSA-2 records followed these steps:

1. File conversion from SSA format to EVT format.
2. File conversion from EVT format to uncorrected acceleration V1 format.
3. File conversion from uncorrected acceleration V1 format to corrected acceleration V2 format. This step includes an instrument and baseline correction, a high-pass filtering of velocity and displacement, and the computation of peak acceleration, velocity, and displacement. The correction method that was selected is the Shakal and Ragsdale method (Shakal and Ragsdale, 1984). The corner frequency used for high-pass filtering varied in the range from 0.12 to 0.20 Hz. The terminal frequency used for low-pass filtering was 45 Hz.
4. File conversion from corrected acceleration V2 format to Fourier and response spectra V3 format. Response spectra were

computed for 5% damping and for periods of 0.3 s and 1.0 s. Specifically, the values of pseudo spectral velocity (PSV) and pseudo spectral acceleration (PSA) were computed. The above periods were selected because they are of interest for earthquake engineering purposes, since these values are spectral periods suggested by the current NEHRP seismic code design guidelines for the assessment of short- and long-period response to strong ground motion (FEMA, 1997). These spectral parameters will also be used later in the attenuation analysis of the 2001 records.

STRONG-MOTION PARAMETERS

Peak values of acceleration and velocity for each component are listed in Tables 4 and 5 for the January 13 and February 13 earthquakes, respectively. Also pseudo spectral acceleration and pseudo spectral velocity are presented. Stations are sorted by increasing source to site distance. The parameters selected for the distance were described previously.

The San Vicente (VI) station recorded the January 13 earthquake, but the record is cut due to an instrument malfunction during the earthquake. The instrument stopped recording during the earthquake due to a power failure in the electrical supply and in the main internal battery. Peak ground acceleration (PGA) values for this cut record are 154.6, 138.2, and 118.2 cm/s^2 for the N-S, vertical, and E-W components, respectively. These values are likely to be lower than the actual PGA because the record envelope and duration appear not to have reached the strongest

TABLE 5. RECORDS FOR FEBRUARY 13, 2001 EARTHQUAKE:
PEAK ACCELERATION, PEAK VELOCITY, AND PSEUDOSPECTRAL VELOCITIES FOR 0.3 s AND 1.0 s

Code	Rupture distance (km)	North-South				Vertical		East-West			
		PGA (cm/s^2)	PGV (cm/s)	PSV T = 0.3 s (cm/s)	PSV T = 1 s (cm/s)	PGA (cm/s^2)	PGV (cm/s)	PGA (cm/s^2)	PGV (cm/s)	PSV T = 0.3 s (cm/s)	PSV T = 1 s (cm/s)
VI	2.5	425	14.6	25.7	8.2	229	4.0	232	6.2	17.7	4.9
BA	12.5	104	25.6	16.2	41.1	121	6.9	139	22.3	18.7	45.6
ZA	15.5	400	20.0	33.9	44.4	257	9.8	296	20.5	35.9	24.7
TO	18.0	238	30	29.9	77.6	235	10.6	246	24.6	33.2	28.5
DB	18.2	98	14.8	13.0	17.3	54	4.6	92	12.2	14.1	21.4
CI	19.3	135	19.9	8.6	10.1	58	3.8	69	8.4	10.4	25.8
PA	20.2	182	7.5	11.3	7.4	44	2.2	105	4.6	6.1	5.0
OB	21.7	105	6.7	12.5	22.6	67	3.3	102	13.9	13.7	10.1
EX	23.1	121	15.2	9.0	19.1	51	2.7	97	6.1	9.9	8.3
VF	24.3	40	3.1	3.3	11.4	31	2.9	39	7.2	2.4	7.9
VS	24.3	76	8.2	5.8	9.0	45	3.5	58	8.7	7.5	14.5
SS	24.9	64	5.7	5.6	11.5	43	2.6	70	10.8	6.0	4.9
UC	25.7	N.D.	N.D.	N.D.	N.D.	39	2.1	57	8.5	8.4	14.5
RF	26.2	42	3.7	4.2	6.9	26	1.8	42	7.4	4.2	7.3
RS	26.2	57	3.9	6.8	8.3	34	2.2	62	8.1	7.5	6.5
QC	27.4	19	6.4	3.9	4.6	17	2.4	26	5.0	2.9	3.9
TE	30.3	46	6.4	2.8	8.7	22	2.0	40	4.8	3.4	6.1
ST	32.6	38	6.4	2.8	7.0	19	2.2	41	7.4	3.2	11.2
BE	34.3	32	4.4	5.3	5.8	30	2.3	70	6.8	6.4	10.9
LI	40.5	90	4.5	12.5	3.7	35	2.4	92	5.0	5.8	3.4
AR	55.1	28	3.2	3.5	4.4	26	1.3	36	1.9	2.7	4.2

Note: Stations ordered with increasing rupture distance. Rupture distance—horizontal distance to surface projection of rupture; PGA—horizontal peak ground acceleration; PGV—horizontal peak ground velocity; PSV—pseudospectral velocity; T—period; N.D.—No data.

part of the shaking, and it was decided not to include it in any part of this study. In addition, there is a record of the February 13 event in San Pedro Nonualco (NO) that was not included in the analysis. In this station, the floor anchor was found broken in the first maintenance visit after this earthquake, presumably due to the very strong shaking (PGA values are 1105.5, 729.4, and 1360.8 cm/s^2 for N-S, vertical, and E-W components, respectively). Figure 4 shows the acceleration time histories of these two records.

Figures 5 and 6 present the observed PGA, PSA, and PSV values versus distance for the January 13 and February 13 earthquakes.

PREDICTION OF STRONG GROUND MOTION PARAMETERS

Regression analysis of the 479 accelerograms was applied to obtain strong ground motion relationships for horizontal PGA, horizontal PSA, and horizontal PSV, for in-slab subduction and shallow upper crustal earthquakes. The number of records for each station is summarized in Table 3.

The total data set comprised 479 triaxial records from 188 earthquakes, of which 61 have their origin in the subduction zone and 127 in the upper crustal faults systems. Table 6 summarizes the parameters characteristics of each subset.

Subduction Earthquakes

Cepeda et al. (1997b) compared a Central American database of 178 subduction earthquake records with the predictions by Alfaro

et al. (1990), Bommer et al. (1996), Crouse (1991), and Youngs et al. (1997), all recent studies of ground motion, which give attenuation estimates specifically for subduction tectonic regimes.

Figure 7A shows the magnitude-distance distribution for the 254 in-slab subduction earthquake records during 2001. The distribution shows a gap in the magnitude range from 5.9 to 7.6 M_w , which is explained by the fact that almost the entire subduction activity of 2001 occurred along the rupture area of the January 13 earthquake, and the energy release associated with this large-magnitude event did not leave conditions for the occurrence of a new large earthquake within the one-year time frame of the present study. This is different from the volcanic chain earthquakes. For example, in Figure 7B, the 6.6 M_w and 5.3 M_w events took place in different fault systems, namely around San Vicente volcano and San Salvador volcano, and in fact, the February 13 earthquake seems to have acted as a trigger for the 5.3 M_w February 17 earthquake (Benito et al., this volume, Chapter 25).

As the magnitude gap in the subduction activity of 2001 includes earthquakes that are important for earthquake engineering purposes, in the present study the attenuation analysis is performed by taking a basic equation that includes earthquakes in the different ranges of magnitudes, and then by making the necessary adjustments to the basic equation for the residuals of the observed strong-motion parameters during 2001.

A recent attenuation equation for in-slab and interface subduction earthquakes is given by Atkinson and Boore (2003), herein referred to as AB03. This equation, which is used here as the basic equation, has been derived by using 1200 records from Japan, Cascadia, Mexico, and Central America, produced

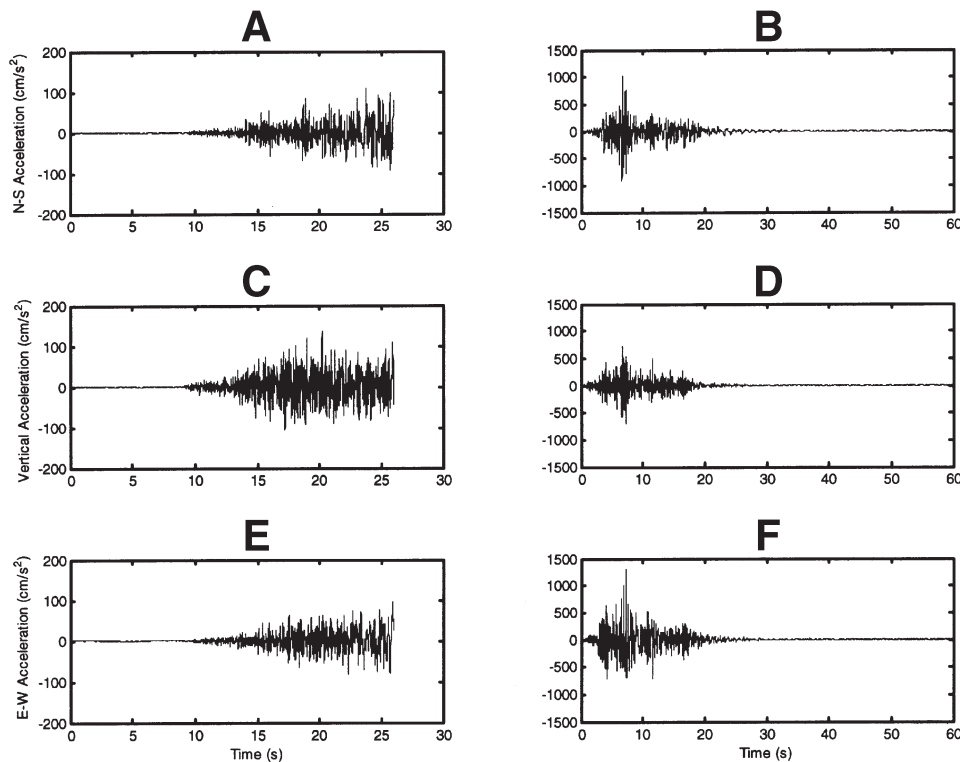


Figure 4. Acceleration time histories of January 13 earthquake record at station VI (left traces, A, C and E) and February 13 earthquake record at station NO (right traces, B, D, and F). A and B: North-south components. C and D: Vertical components. E and F: East-west components.

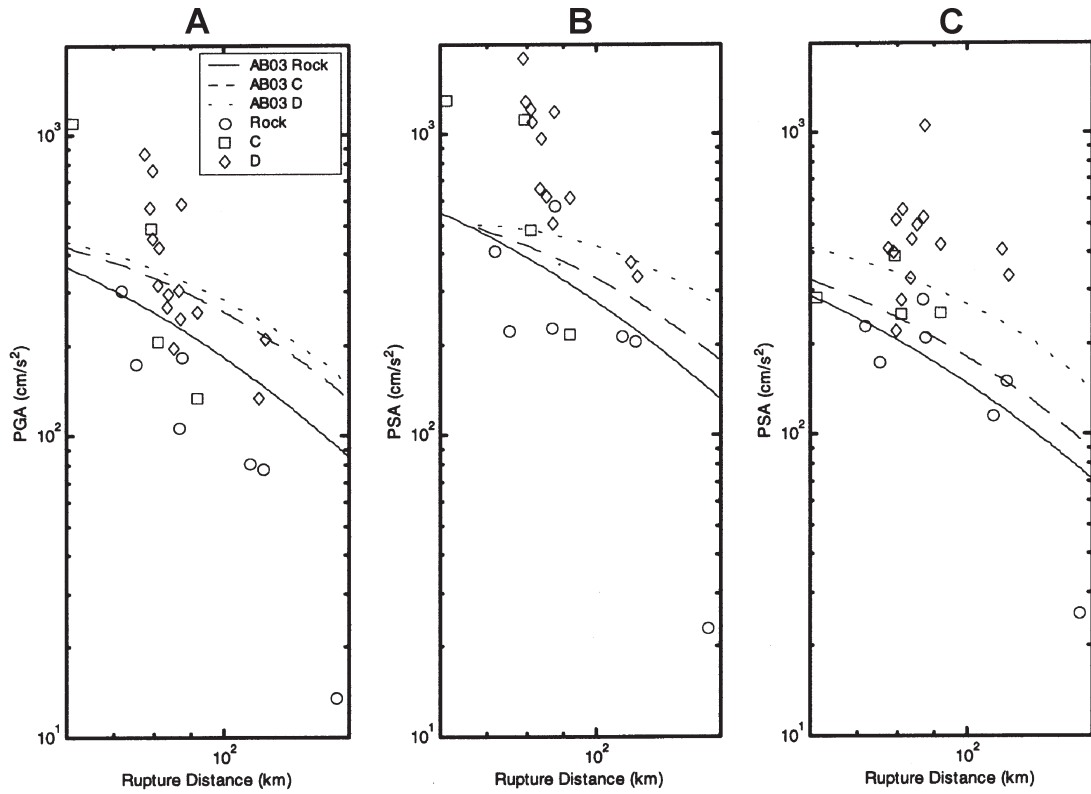


Figure 5. Comparison of observed strong-motion parameters for January 13 earthquake to predicted attenuation curves by Atkinson and Boore (2003). For the observed values, only the largest component is shown. A: Peak ground acceleration. B: Pseudo spectral acceleration for 0.3 s. C: Pseudo spectral acceleration for 1.0 s. AB03—Atkinson and Boore (2003). Circles—rock sites. Squares—NEHRP C sites. Diamonds—NEHRP D sites.

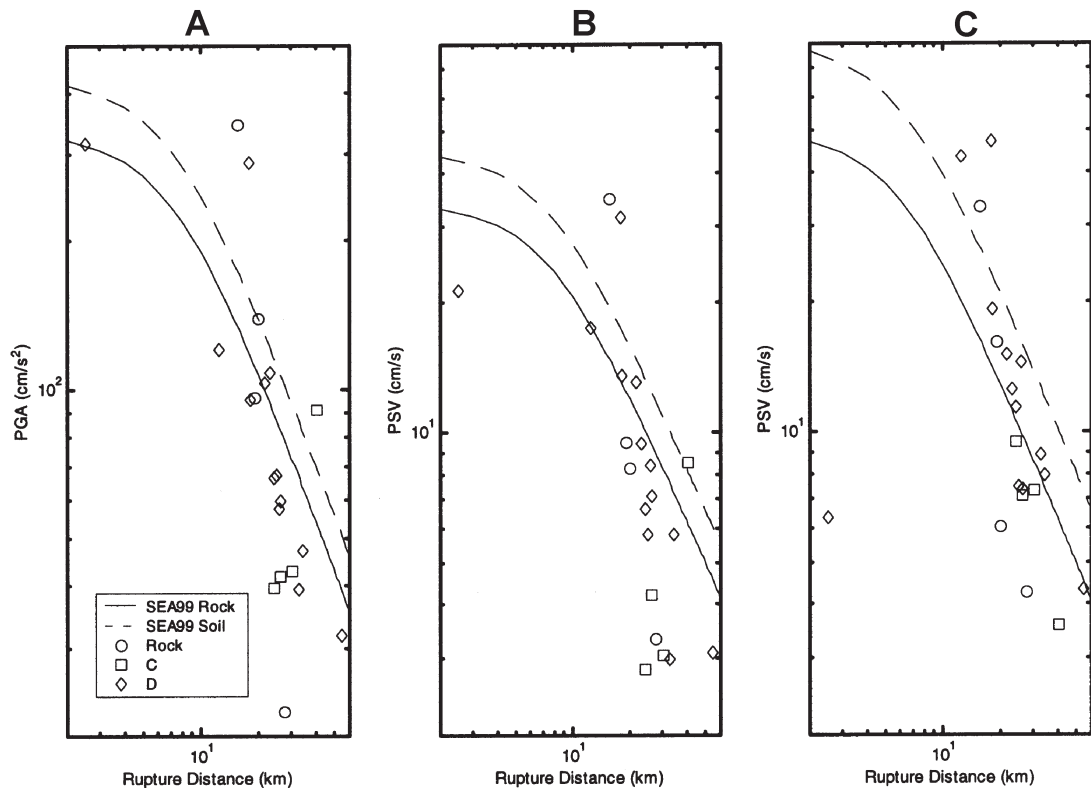


Figure 6. Comparison of observed strong-motion parameters for February 13 earthquake to predicted attenuation curves by Spudich et al. (1999). Observed values are geometric mean. A: Peak ground acceleration. B: Pseudo spectral velocity for 0.3 s. C: Pseudo spectral velocity for 1.0 s. SEA99—Spudich et al. (1999). Circles—rock sites. Squares—NEHRP C sites. Diamonds—NEHRP D sites.

TABLE 6. SUMMARY OF CHARACTERISTICS OF DATABASE USED IN ATTENUATION ANALYSIS

Type of event	Number of earthquakes	NEHRP D site records	NEHRP C site records	Rock site records	Total records	M_{\min}	M_{\max}	h_{\min} (km)	h_{\max} (km)	r_{\min} (km)	r_{\max} (km)
Subduction	61	153	60	41	254	2.8	7.7	26.1	111.8	57.5*	190.2*
Shallow upper crustal	127	160	21	44	225	2.4	6.6	1.9	26.4	0.4#	102.8#
Total	188	313	81	85	479	N.A.	N.A.	N.A.	N.A.	N.A.	N.A.

Note: M_{\min} —minimum moment magnitude; M_{\max} —maximum moment magnitude; h_{\min} —minimum focal depth; h_{\max} —maximum focal depth; r_{\min} —minimum rupture distance; r_{\max} —maximum rupture distance.

*distance to plane of rupture for events with large magnitudes or hypocentral distance for low and moderate magnitude events.

#horizontal distance to surface projection of rupture for events with large magnitudes or epicentral distance for low and moderate magnitude events.

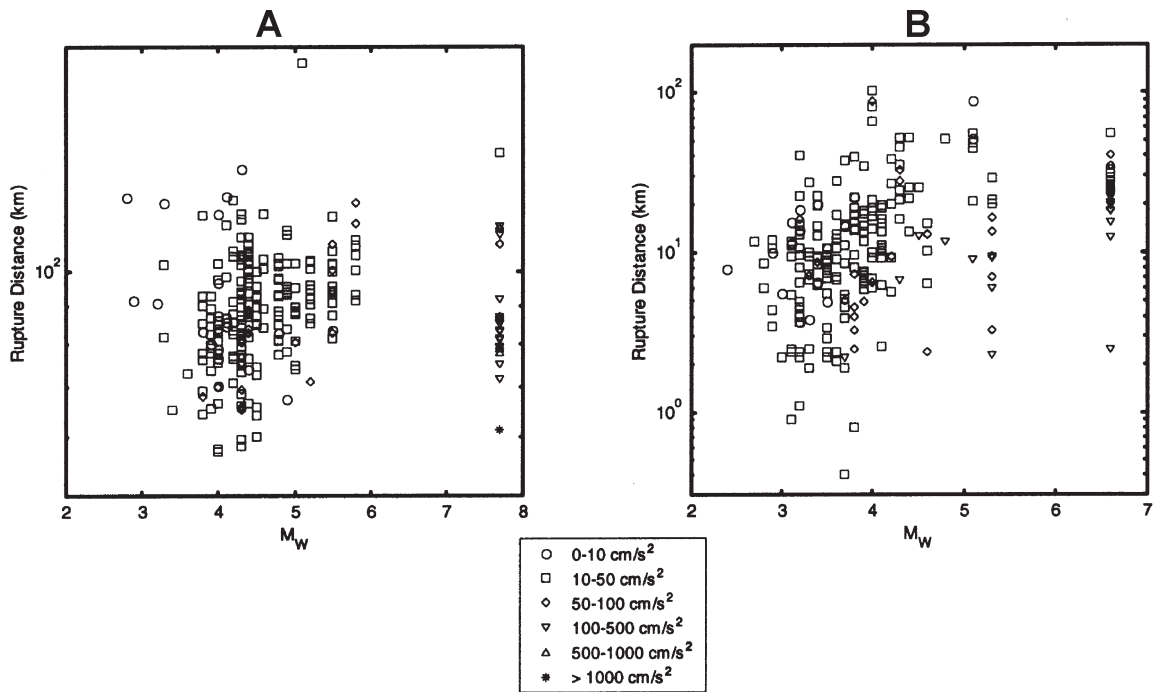


Figure 7. Magnitude-distance distribution for subduction earthquake records (A) and shallow upper crustal earthquake records (B). Marker types are classified by range of horizontal peak ground acceleration.

by more than 500 earthquakes of moment magnitude 5 to 8.3 recorded within 300 km. The equation has the following form:

$$\log Y = C_1 + C_2 M + C_3 h + C_4 R - g \log R + C_5 sl S_C + C_6 sl S_D + C_7 sl S_E \quad (2)$$

in which Y is peak ground acceleration (PGA) or 5% damped pseudo spectral acceleration (PSA) in cm/s^2 , using the random horizontal component; in this study, the larger component will be used. M is moment magnitude; h is focal depth in km; $R = \sqrt{D_{\text{fault}}^2 + \Delta^2}$, in which D_{fault} is the closest distance to the

fault rupture surface, in km; in this study, D_{fault} is the hypocentral distance for all events other than the January 13 earthquake; $\Delta = 0.00724 (10^{0.507 M})$; $S_C = 1$ for NEHRP C soils, or 0 otherwise; $S_D = 1$ for NEHRP D soils, or 0 otherwise; $S_E = 1$ for NEHRP E soils, or 0 otherwise; $g = 10^{(0.301-0.01M)}$ for in-slab events; $sl = 1$ for $PGA_{rx} \leq 100 \text{ cm/s}^2$ or frequency $f \leq 1 \text{ Hz}$; $sl = 1 - (f-1)(PGA_{rx} - 100)/400$ for $100 < PGA_{rx} < 500 \text{ cm/s}^2$ ($1 \text{ Hz} < f < 2 \text{ Hz}$); $sl = 1 - (f-1)$ for $PGA_{rx} \geq 500 \text{ cm/s}^2$ ($1 \text{ Hz} < f < 2 \text{ Hz}$); $sl = 1 - (PGA_{rx} - 100)/400$ for $100 < PGA_{rx} < 500 \text{ cm/s}^2$ ($f \geq 2 \text{ Hz}$); $sl = 0$ for $PGA_{rx} \geq 500 \text{ cm/s}^2$ ($f \geq 2 \text{ Hz}$); PGA_{rx} is the predicted PGA on rock (NEHRP B site) in cm/s^2 .

Table 7 presents the regression coefficients and standard deviations in the original AB03 equations and in the adjusted forms of the equations. The standard deviations in the original AB03 equations are the values reported by Atkinson and Boore (2003), whereas the standard deviations in the adjusted equations are calculated from the residuals of the records in 2001. The coefficients for PSA at a period of 0.3 s have been interpolated from the original coefficients given in the AB03 equations at periods of 0.2 s and 0.4 s. The interpolation has been performed assuming that there is a linear variation of $\log(\text{PSA})$ versus $\log(\text{frequency})$.

Figure 5 shows the predicted curves from AB03 for the January 13 earthquake along with the observed strong-motion parameters. In this plot it is interesting to see the behavior of the La Libertad (LI) station. LI is the closest station to the rupture surface and seems to be in the rupture direction (central station in the coast in Fig. 2). Consistently, this station shows a large underestimation for PGA (Fig. 5A) and for high-frequency PSA (Fig. 5B), whereas for low-frequency PSA (Fig. 5C) the predicted value agrees closely with the observed PSA. This high-frequency response was also observed by Bommer et al. (2002) when they showed the acceleration response spectrum for this station. A sharp high-frequency response seems to be also a local characteristic of LI, as it was presented by Bommer et al. (1997) for a moderate-magnitude subduction earthquake.

Figures 8A and 8B show the distribution of residuals in terms of magnitude and distance for PGA using AB03. The residuals are also classified by distance and magnitude, respectively. Figure 8A shows a clear linear dependence on magnitude, whereas observation of Figure 8B indicates an underestimation of PGA, without any dependence on distance. The underestimation is larger as the magnitude becomes smaller. The adjustment was performed to the constant term C_1 and the magnitude coefficient C_2 . Figures 8C and 8D present the distribution of residuals after the adjustment of the coefficients. The fit of the observed 2001 data is similar to the database of the original AB03 equation, which is apparent when the adjusted standard deviation of

0.26 is compared to the slightly higher value of 0.27 reported by Atkinson and Boore (2003).

The distributions of residuals for PSA at periods of 0.3 s and 1.0 s are presented in Figures 9 and 10. Note the similarities of the distribution of residuals in Figures 9A and 10A compared to Figure 8A. The dependence on magnitude follows the same trend, even though the underestimation for low magnitudes is higher in PSA than in PGA. As in the case of the adjustment of the PGA equation, the coefficients that were modified are the constant term C_1 and the magnitude coefficient C_2 . The standard deviations increase in the adjusted equations compared with the original AB03 equations.

An interesting observation from Table 7 is the trend of the adjustments in the C_1 and C_2 regression coefficients toward the coefficients for interface events. For example, the constant term in AB03 for PGA is -0.04713 , and after the adjustment C_1 is 2.93078. This value is close to the coefficient 2.991 for interface events in the AB03 equation. A similar trend appears in the magnitude coefficient of 0.6909 for AB03 in-slab events and the smaller adjusted coefficient of 0.2877, compared to the AB03 coefficient of 0.03525 for interface events. These trends are also observed in the case of the coefficients for PSA. These observations impose a question about the type of the subduction events in the El Salvador database. Based on the focal mechanisms and the tectonics of the region, in-slab-type subduction earthquakes were assumed in the present analysis. However, it may be interesting in future studies to make an assessment and a revision of the location of earthquakes within the subduction area in the surroundings of El Salvador.

Shallow Upper Crustal Earthquakes

Analysis of attenuation for shallow upper crustal earthquakes in Central America has been also performed by Cepeda et al. (1997b). They compared a database of 116 Central American shallow crustal earthquake records with the estimates of Alfaro et al. (1990), Ambraseys et al. (1996), and Spudich et al. (1997).

TABLE 7. REGRESSION COEFFICIENTS AND STANDARD DEVIATIONS IN ATTENUATION EQUATIONS FOR IN-SLAB SUBDUCTION EVENTS

Strong motion parameter	Attenuation equation	C_1	C_2	C_3	C_4	C_5	C_6	σ
PGA	AB03	-0.04713	0.6909	0.01130	-0.00202	0.19	0.24	0.27
PGA	AB03 after adjustments	2.93078	0.2877	N.A.	N.A.	N.A.	N.A.	0.26
PSA (T = 0.3 s)	AB03*	0.2173	0.73915	0.00339	-0.00184	0.14	0.33	0.28 [#]
PSA (T = 0.3 s)	AB03 after adjustments	3.31445	0.34496	N.A.	N.A.	N.A.	N.A.	0.32
PSA (T = 1 s)	AB03	-1.02133	0.8789	0.00130	-0.00173	0.10	0.30	0.29
PSA (T = 1 s)	AB03 after adjustments	1.85185	0.51846	N.A.	N.A.	N.A.	N.A.	0.33

Note: C_1 , C_2 , C_3 , C_4 , C_5 and C_6 —regression coefficients; σ —standard deviation of residuals; PGA—horizontal peak ground acceleration (cm/s^2); PSA—horizontal pseudo spectral acceleration (cm/s^2); T—period; AB03—Atkinson and Boore (2003); N.A.—not applicable, coefficient not adjusted.

* linearly interpolated from Atkinson and Boore (2003) using regression coefficients for T = 0.2 s and T = 0.4 s.

standard deviation in Atkinson and Boore (2003) for T = 0.2 s and T = 0.4 s.

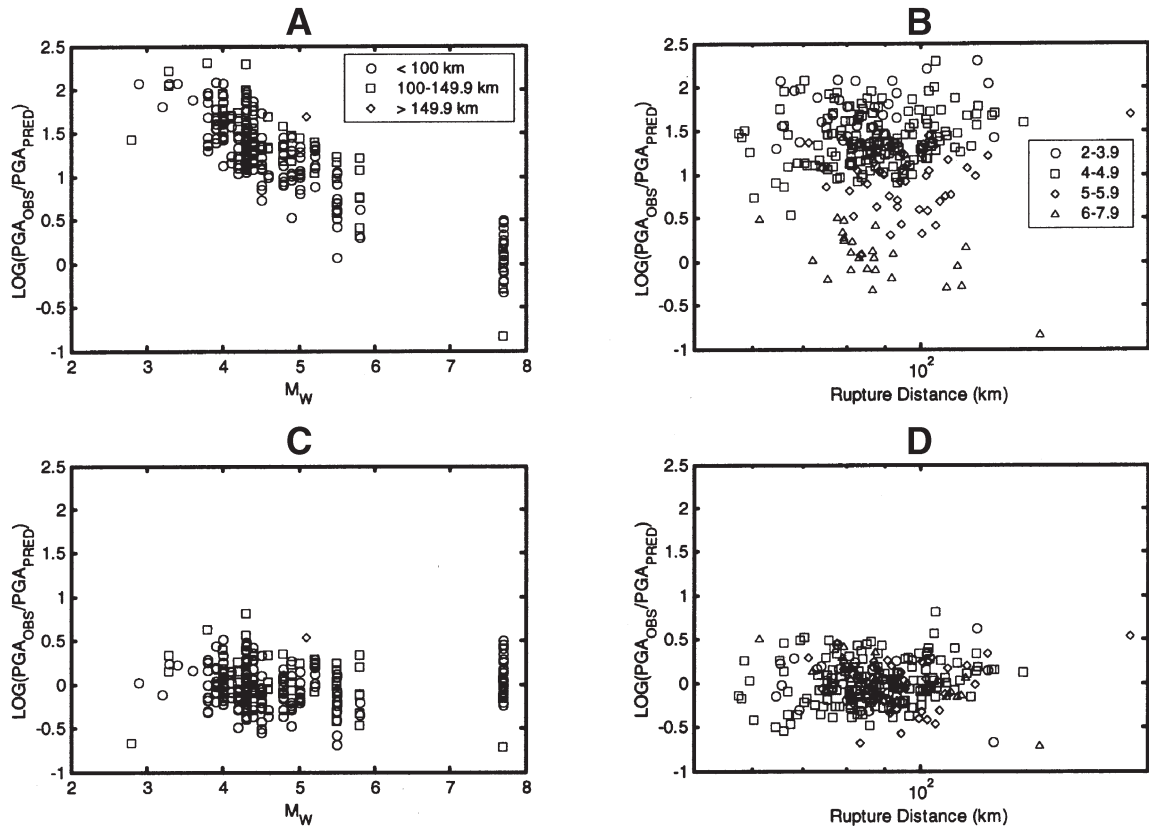


Figure 8. Distribution of residuals of peak ground acceleration versus magnitude (A) and distance (B) for the AB03 equation (Atkinson and Boore, 2003) using subduction earthquake records. C and D: Distributions of adjusted residuals.

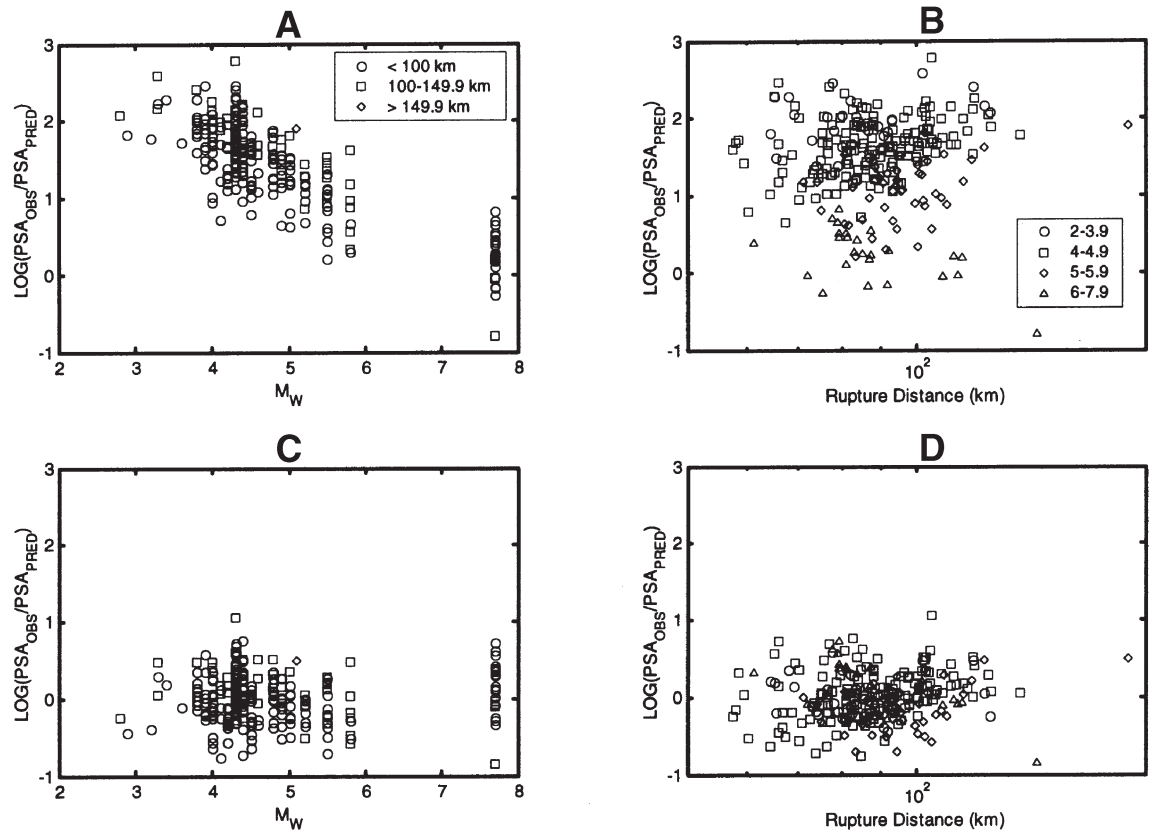


Figure 9. Distribution of residuals of pseudo spectral acceleration (period = 0.3 s) versus magnitude (A) and distance (B) for the AB03 equation (Atkinson and Boore, 2003) using subduction earthquake records. C and D: Distributions of adjusted residuals.

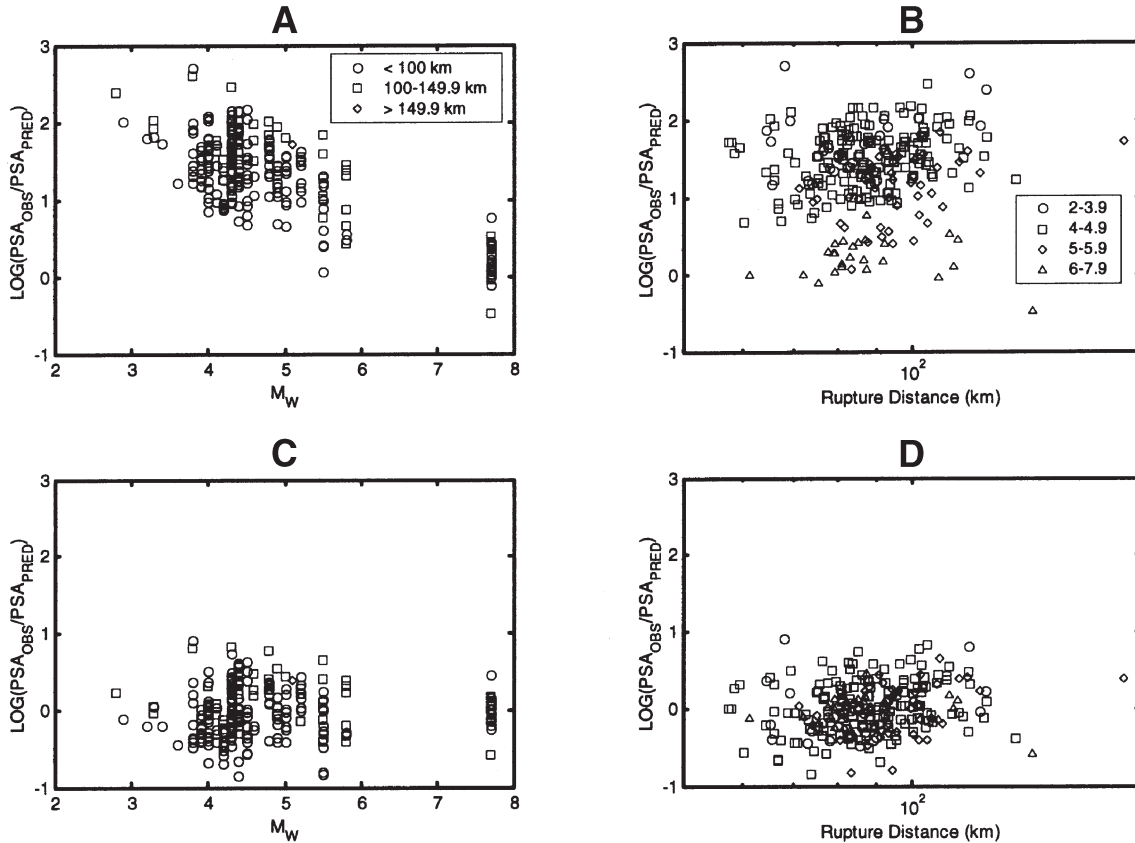


Figure 10. Distribution of residuals of pseudo spectral acceleration (period = 1.0 s) versus magnitude (A) and distance (B) for the AB03 equation (Atkinson and Boore, 2003) using subduction earthquake records. C and D: Distributions of adjusted residuals.

Figure 7B shows the magnitude-distance distribution for the shallow upper crustal records of 2001 classified according to horizontal PGA. The distribution covers most of the magnitude ranges, except in the range from 5.4 to 6.5 M_w .

As the above gap of magnitudes includes damaging earthquakes of interest for earthquake engineering purposes, the database is not complete, and in this study it is not considered appropriate to derive an attenuation equation based solely on these data. The preferred approach is to use an existing attenuation equation and make the necessary adjustments based on the distribution of the residuals of the observed data.

The Spudich et al. (1999) equation, SEA99, is used as the base for the analysis. This relation was developed based on 142 strong-motion records from 39 extensional regime earthquakes in the United States, Central America, Italy, Mexico, Greece, New Zealand, Turkey, and Holland. The original equation is directly applicable to earthquakes with moment magnitudes in the range of 5.0–7.7 and with source-site distances less than 70 km.

The SEA99 equation has this form:

$$\log Y = B_1 + B_2(M - 6) + B_3(M - 6)^2 + B_5 \log r + B_6 \Gamma \quad (3)$$

in which Y is PGA (in g) or pseudovelocity response (cm/s) at 5% damping for the geometric mean horizontal component of motion; B_1 to B_6 are the regression coefficients; M is moment magnitude; $r = \sqrt{r_{jb}^2 + H^2}$, in which r_{jb} is the closest horizontal distance (km) to the vertical projection of the rupture; in this study, r_{jb} is equal to the epicentral distance for all earthquakes, except in the case of the February 13 earthquake; H is a regression value; $\Gamma = 0$ for rock and $\Gamma = 1$ for soil.

Table 8 lists the regression coefficients and standard deviations in the original SEA99 equations and in the adjusted versions of the equations. The standard deviations in the original SEA99 equations are the values reported by Spudich et al. (1999), whereas the standard deviations in the adjusted forms are calculated from the residuals of the records in 2001.

Figure 6 shows the predicted attenuation curves by SEA99 for the February 13 earthquake along with the observed strong-motion parameters. In this case, the closest station to the fault is the San Vicente, VI, station (leftmost diamond in Fig. 6). The directivity effect at VI that was previously discussed by Cepeda (2001b) is also apparent in the variation of the observed PGA and PSV. It can be seen that PGA (Fig. 6A) and PSV at high

TABLE 8. REGRESSION COEFFICIENTS AND STANDARD DEVIATIONS
IN ATTENUATION EQUATIONS FOR SHALLOW UPPER-CRUSTAL EVENTS

Strong motion parameter	Attenuation equation	B_1	B_2	B_3	B_5	B_6	H	σ
PGA	SEA99	0.299	0.229	0	-1.052	0.112	7.27	0.203
PGA	SEA99 after adjustments	-0.0423	N.A.	N.A.	N.A.	N.A.	N.A.	0.288
PSV (T = 0.3 s)	SEA99	2.263	0.334	-0.070	-1.020	0.121	7.72	0.232
PSV (T = 0.3 s)	SEA99 after adjustments	2.270	N.A.	N.A.	N.A.	N.A.	N.A.	0.347
PSV (T = 1 s)	SEA99	2.276	0.450	-0.014	-1.083	0.210	6.01	0.269
PSV (T = 1 s)	SEA99 after adjustments	0.6949	N.A.	N.A.	-0.0585	N.A.	N.A.	0.370

Notes: B_1 , B_2 , B_3 , B_5 and B_6 —regression coefficients; H—regression value used for calculation of the distance term in the attenuation equation; σ —standard deviation of residuals; PGA—peak ground acceleration (cm/s^2) for the geometric mean horizontal component; PSV—pseudo spectral velocity (cm/s) for the geometric mean horizontal component; T—period; SEA99—Spudich et al. (1999); N.A.—not applicable, coefficient not adjusted.

frequencies (Fig. 6B) have a close agreement with the predicted values. However, PSV at low frequencies (Fig. 6C) is significantly overestimated, which can be partially explained by the effects of the rupture directivity at this station. At San Bartolo station, BA, which is the second closest station to the fault (second leftmost diamond in Fig. 6), the observed strong-motion parameters also show an apparent effect of the rupture directivity, but this time for a station that is opposite to the direction of rupture propagation. For PGA (Fig. 6A) a slight overestimation is seen from the SEA99 attenuation curves. This overestimation is reduced for the high-frequency PSV (Fig. 6B). However, for the low-frequency PSV (Fig. 6C), the SEA99 equation predicts an underestimated value. These observations are an indication of the rupture directivity effects at BA, which are producing amplitudes that are large for the low-frequency contents of the signal and small for the high-frequency response.

Figure 11 shows the distributions of residuals for observed PGA in terms of magnitude and distance, and grouped in classes. Figures 11A and 11B show the residuals calculated from the original SEA99 equation. The trend of the data in these figures indicates some overestimation by the SEA99 equation. This overestimation does not have a clear dependence on magnitude (Fig. 11A). There is a slight dependence on distance in Figure 11B. This variation is small compared to the scatter of the residuals. After making an adjustment of the constant term B_1 , Figures 11C and 11D present the distribution of residuals in the adjusted version of the SEA99 equation.

In the case of the observed pseudo spectral velocity values for a period of 0.3 s, Figures 12A and 12B show that there is a balanced distribution of overestimations and underestimations. Again, there seems to be no clear dependence on magnitude or distance. After adjusting the constant term B_1 , Figures 12C and 12D present the distribution of residuals in the adjusted form of the SEA99 equation. The constant term in Table 8 shows a slight increase from

the original 2.263 to the adjusted 2.270, which is an indication that the original SEA99 is only making a small underestimation.

The observed pseudo spectral velocities for a period of 1.0 s are generally lower than the predicted values, as it is shown in Figures 13A and 13B. Some trend in the distribution in terms of distance is present in Figure 13B. In this case, the regression was adjusted in the constant term B_1 and in the distance coefficient B_5 . Figures 13C and 13D present the distribution of residuals. Note the significant increase in the distance coefficient B_5 after making the adjustments: from -1.083 to -0.0585. This is an indication of a low geometrical spreading attenuation of the low-frequency contents of the strong ground motion.

DISCUSSION

Our estimates of attenuation for shallow upper crustal and subduction earthquakes have a number of aspects that deserve further study and review. Firstly, it is necessary to collect more records from moderate-magnitude events in order to complete the magnitude-distance distribution, particularly in the range of M_w 5.9 to 7.6 for subduction earthquakes and M_w 5.4 to 6.5 for shallow upper crustal events. Secondly, the attenuation characteristics of the 2001 subduction earthquakes show a closer agreement with the characteristics of interface-type events rather than with the assumed in-slab type. This observation suggests the necessity of further studies of the type of subduction earthquakes in the surroundings of El Salvador. In a third aspect, the ground motion attenuation for the February 13 earthquake shows some indication of the effects of rupture directivity. Bommer et al. (2001) also identified rupture directivity effects in the strong-motion recordings from an earlier upper crustal earthquake in 1986. These observations indicate that this effect should have proper consideration at least in the development of site-specific earthquake hazard assessments. Finally, the fact that geologic site

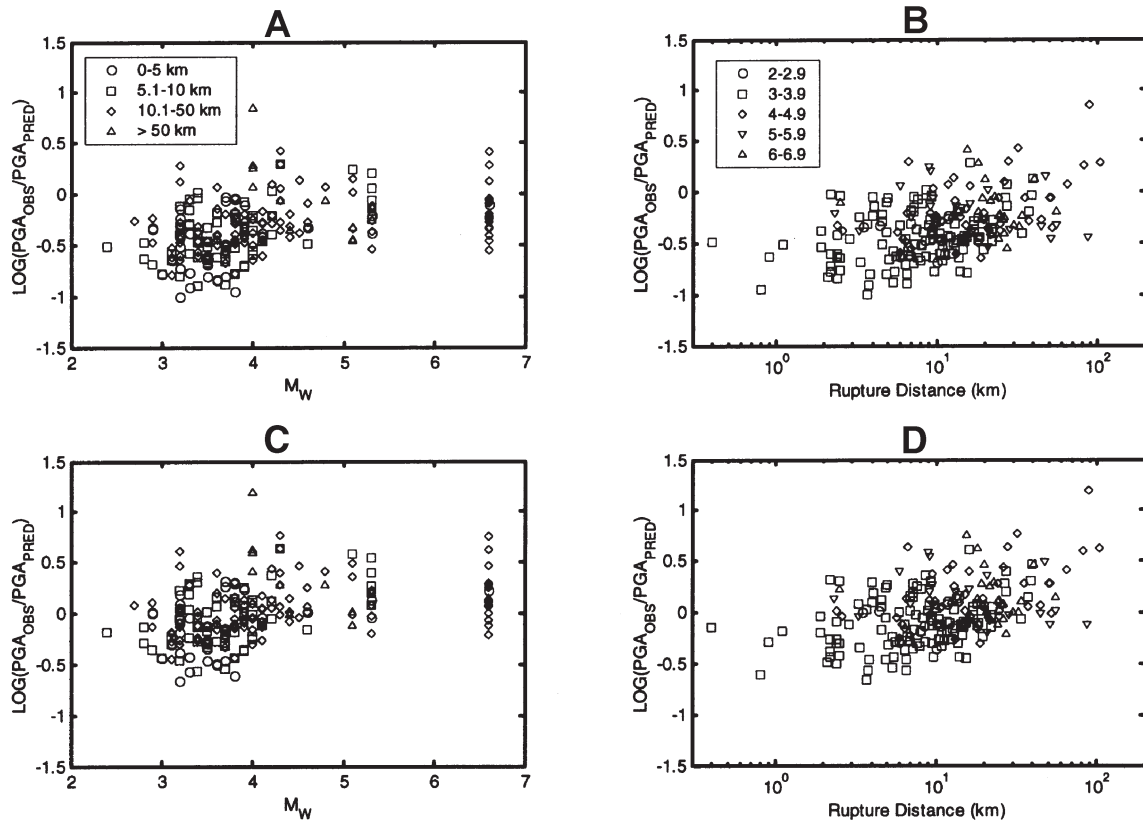


Figure 11. Distribution of residuals of peak ground acceleration versus magnitude (A) and distance (B) for the SEA99 equation (Spudich et al., 1999) using shallow upper crustal earthquake records. C and D: Distributions of adjusted residuals.

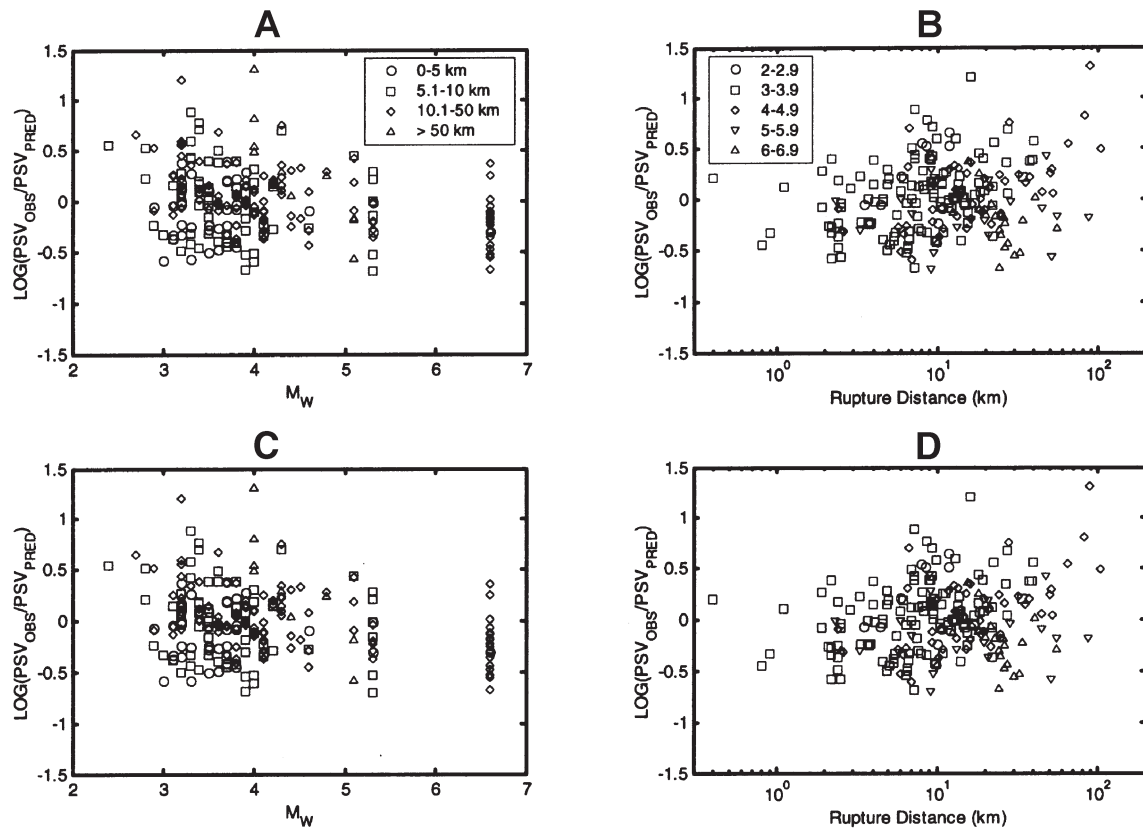


Figure 12. Distribution of residuals of pseudo spectral velocity (period = 0.3 s) versus magnitude (A) and distance (B) for the SEA99 equation (Spudich et al., 1999) using shallow upper crustal records. C and D: Distributions of adjusted residuals.

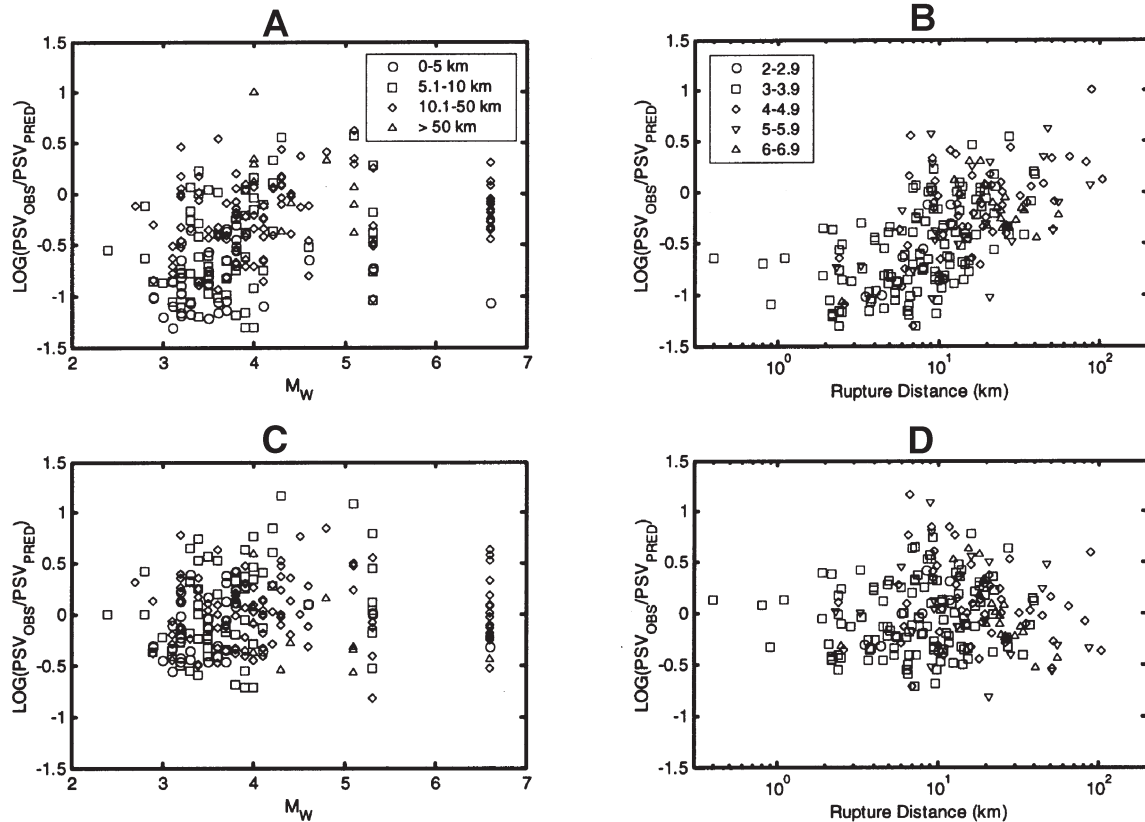


Figure 13. Distribution of residuals of pseudo spectral velocity (period = 1.0 s) versus magnitude (A) and distance (B) for the SEA99 equation (Spudich et al., 1999) using shallow upper crustal earthquake records. C and D: Distributions of adjusted residuals.

conditions are known in detail for only 2% of the strong-motion database is a clear indication that the task of performing detailed site investigations at every station is urgent in order to establish site classes more reliably.

ACKNOWLEDGMENTS

Our colleagues from SNET (Servicio Nacional de Estudios Territoriales) have provided very helpful assistance in the provision of the necessary seismological, strong-motion, and geotechnical data in the SNET stations. Special thanks to Manuel Díaz, Douglas Hernández, and Griselda Marroquín. Their comments and exchange of ideas have also been an invaluable resource for our study. Carlos Pullinger from SNET and Patricia de Hasbun from UCA (Universidad Centroamericana “José Simeón Cañas”) have devoted their interest and efforts to strengthen the interinstitutional bonds between SNET, UPM (Universidad Politécnica de Madrid), and UCA.

José Rivas from GESAL (Geotérmica Salvadoreña) kindly provided the records and information from their seismological network in Berlín, Usulután.

David Boore from the U.S. Geological Survey and Conrad Lindholm from NORSAR provided very useful comments after their in-depth and rigorous revisions. The attenuation analysis for the spectral ordinates was suggested by David Boore. Julian Bommer from Imperial College London also provided very detailed and rigorous observations that greatly improved the contents of this paper.

REFERENCES CITED

- Alfaro, C.S., Kiremidjian, A.S., and White, R.A., 1990, Seismic zoning and ground motion parameters for El Salvador: The John A. Blume Earthquake Engineering Center Report No. 93, Palo Alto, California, Stanford University, 157 p.
- Ambraseys, N.N., Simpson, K.A., and Bommer, J.J., 1996, Prediction of horizontal response spectra in Europe: *Earthquake Engineering and Structural Dynamics*, v. 25, p. 371–400.
- Atkinson, G.M., and Boore, D.M., 2003, Empirical ground-motion relations for subduction-zone earthquakes and their application to Cascadia and other regions: *Bulletin of the Seismological Society of America*, v. 93, no. 4, p. 1703–1729.
- Benito, M.B., Cepeda, J.M., and Martínez Díaz, J.J., 2004, Analysis of the spatial and temporal distribution of the 2001 earthquakes in El Salvador, *in* Rose, W.I., et al., eds., *Natural hazards in El Salvador*: Boulder, Colorado, Geological Society of America Special Paper 375, p. 339–356 (this volume).

- Bommer, J.J., Hernández, D.A., Navarrete, J.A., and Salazar, W.M., 1996, Seismic hazard assessments for El Salvador: *Geofísica Internacional*, v. 35, p. 227–244.
- Bommer, J.J., Udías, A., Cepeda, J.M., Hasbun, J.C., Salazar, W.M., Suárez, A., Ambraseys, N.N., Buforn, E., Cortina, J., Madariaga, R., Méndez, P., Mezcuá, J., and Papastamatiou, D., 1997, A new digital accelerograph network for El Salvador: *Seismological Research Letters*, v. 68, p. 426–437.
- Bommer, J.J., Georgallides, G., and Tromans, I.J., 2001, Is there a near-field for small-to-moderate magnitude earthquakes?: *Journal of Earthquake Engineering*, v. 5, no. 3, p. 395–423.
- Bommer, J., Benito, B., Ciudad-Real, M., Lemoine, A., López-Menjívar, M., Madariaga, R., Mankelov, J., Méndez de Hasbun, P., Murphy, W., Nieto-Lovo, M., Rodríguez-Pineda, C.E., and Rosa, H., 2002, The El Salvador earthquakes of January and February 2001: Context, characteristics, and implications for seismic risk: *Soil Dynamics and Earthquake Engineering*, v. 22, p. 389–418.
- Brizuela, B., and Menjívar, L., 2001, *Sistemas de información geográfica en el manejo de peligros naturales* [B.S. thesis]: Universidad Centroamericana “José Simeón Cañas,” El Salvador, 184 p.
- Cepeda, J.M., 2001a, Información acelerográfica de los terremotos del 13 de enero y 13 de febrero de 2001: *Revista Asociación Salvadoreña de Ingenieros y Arquitectos*, March, no. 139, p. 28–33.
- Cepeda, J.M., 2001b, Ciento cincuenta días después del 13 de enero y 15 años después del 10 de octubre: algunas consideraciones técnicas sobre los sismos y sus efectos: *Revista Estudios Centroamericanos, ECA*, v. 631–632, p. 459–472.
- Cepeda, J.M., Salazar, W.M., and Bommer, J.J., 1997a, Caracterización de la red acelerográfica “Talulin,” in Méndez de Hasbun, P., and Hasbun, J.C., eds., *Proceedings, Seminar for the Assessment and Mitigation of Seismic Risk in Central America*, San Salvador, El Salvador, p. 109–118.
- Cepeda, J.M., Salazar, W.M., and Bommer, J.J., 1997b, Ecuaciones de atenuación para Centroamérica: I. Aceleración máxima del terreno, in Méndez de Hasbun, P., and Hasbun, J.C., eds., *Proceedings, Seminar for the Assessment and Mitigation of Seismic Risk in Central America*, San Salvador, El Salvador, p. 119–128.
- Crouse, C.B., 1991, Ground-motion attenuation equations for earthquakes on the Cascadian subduction zone: *Earthquake Spectra*, v. 7, p. 201–236.
- Dobry, R., Borcherdt, R., Crouse, C., Idriss, I., Joyner, W., Martin, G., Power, M., Rinne, E., and Seed, R., 2000, New site coefficients and site classification system used in recent building seismic code provisions: *Earthquake Spectra*, v. 16, p. 41–67.
- FEMA, 1997, NEHRP recommended provisions for seismic regulations for new buildings and other structures: FEMA 302, Federal Emergency Management Agency, Washington, D.C., 335 p.
- Italtekna-Italconsult, 1987, *Valutazione della pericolosità sismica nelle aree del Distretto Sanitario A3 (San Salvador) e del Distretto 7 (Apopa). Parte 4ª—studi di risposta sismica locale ed elaborazione delle carte di Ricostruzione*, Repubblica Italiana, Ministero degli Affari Esteri, Direzione Generale per la Cooperazione allo Sviluppo, 300 p.
- Lay, T., and Wallace, T.C., 1995, *Modern global seismology*: San Diego, California, Academic Press, 521 p.
- Shakal, A.F., and Ragsdale, J.T., 1984, Acceleration, velocity and displacement noise analysis for the CSMIP accelerogram digitization system, in *Proceedings, 8th World Conference on Earthquake Engineering*, San Francisco, v. 2, p. 111–118.
- Spudich, P., Fletcher, J.B., Hellweg, M., Boatwright, J., Sullivan, C., Joyner, W.B., Hanks, T.C., Boore, D.M., McGarr, A., Baker, L.M., and Lindh, A.G., 1997, SEA 96—A new predictive relation for earthquake ground motions in extensional tectonic regimes: *Seismological Research Letters*, v. 68, p. 190–198.
- Spudich, P., Joyner, W.B., Lindh, A.G., Boore, D.M., Margaris, B.M., and Fletcher, J.B., 1999, SEA 99—A revised ground motion prediction relation for use in extensional tectonic regimes: *Bulletin of the Seismological Society of America*, v. 89, no. 5, p. 1156–1170.
- Wells, D.L., and Coppersmith, K.J., 1994, New empirical relationships among magnitude, rupture length, rupture width, rupture area and surface displacement: *Bulletin of the Seismological Society of America*, v. 84, no. 4, p. 974–1002.
- Youngs, R.R., Chiou, S.J., Silva, W.J., and Humphrey, J.R., 1997, Strong motion attenuation relationships for subduction zone earthquakes: *Seismological Research Letters*, v. 68, p. 58–73.

MANUSCRIPT ACCEPTED BY THE SOCIETY JUNE 16, 2003

